Active Contour Model driven by Globally Signed Region Pressure Force

Mohammed M. Abdelsamea and Sotirios A. Tsaftaris
IMT Institute for Advanced Studies, Piazza S. Ponziano, 6, 55100 Lucca, Italy
mohammed.abdelsamea@imtlucca.it; s.tsaftaris@imtlucca.it

***Abstract*—One of the most popular and widely used global active contour models (*ACM*) is the region-based ACM, which relies on the assumption of homogeneous intensity in the regions of interest. As a result, most often than not, when images violate this assumption the performance of this method is limited. Thus, handling images that contain foreground objects characterized by multiple intensity classes present a challenge. In this paper, we propose a novel active contour model based on a new Signed Pressure Force (*SPF*) function which we term Globally Signed Region Pressure Force (*GSRPF*). It is designed to incorporate, in a global fashion, the skewness of the intensity distribution of the region of interest (*ROI*). It can accurately modulate the signs of the pressure force inside and outside the contour, it can handle images with multiple intensity classes in the foreground, it is robust to additive noise, and offers high efficiency and rapid convergence. The proposed *GSRPF* is robust to contour initialization and has the ability to stop the curve evolution close to even ill-defined (weak) edges. Our model provides a parameter-free environment to allow minimum user intervention, and offers both local and global segmentation properties. Experimental results on several synthetic and real images demonstrate the high accuracy of the segmentation results in comparison to other methods adopted from the literature.**

***Index Terms*—region-based segmentation; variational level set method; active contours; signed pressure force**

I. Introduction

One of the most known approaches to object segmentation are active contour methods. Overall, such models can be categorized into three categories: edge-based, region-based and hybrid models that combine the advantages of both edge and regional information. One of the most popular edge-based models is the geodesic active contours (*GAC*) model, first proposed in [1]. This model, and its many variants, uses an edge-detector, usually the gradient of the image, to stop the initial contour on the boundary of the objects of interest [1]–[7]. As a result, the model has the ability to handle well images with well-defined edge information; however, when images have a high level of noise or the object is characterized by weak edges, they cannot converge at the right boundaries.

An alternate approach, the Chan-Vese active contours ($C-V$) model [8], is one of the most common region-based models. The main idea behind this kind of model is to use a region's statistical intensity information to construct a stopping function that can stop the contour evolution among different regions. Compared to edge-based models, the region-based model usually performs better in images with blurred edges and is less sensitive to the contour initialization. However, by design, this model assumes a certain characteristic shape for the intensity distribution for the foreground and background.

A model that combines the advantages of the edge-based and region-based models is the Geodesic-Aided Chan-Vese (*GACV*) model [9]. This hybrid model includes region and edge information in its level set flow function. Thus, it can selectively adjust to local or global segmentation. Zhang et al. [10] proposed a region-based active contour model (*ACM*). It utilizes statistical information inside and outside the contour to construct a region-based signed pressure force (*SPF*) function, which is able to better control the direction of evolution. However, both models still assume a Gaussian intensity within the ROI.

Several authors have considered to introduce terms that relate to local and global intensity information in the SPF function to handle additional intensity classes and image inhomogeneity [11]–[14]. However, these models are sensitive to contour initialization and additive noise of high strength. Furthermore, when the contour is close to the object boundaries, the influence of the global intensity force may distract the contour from the real object boundary, leading to object leaking [15].

It is evident that global models cannot accommodate objects that are constituted of more than one intensity classes and on the other hand local models although they may be able to handle such occasions, they are sensitive to initialization and may lead to leaking.

In this paper, motivated by these observations we propose a new energy formulation that incorporates higher order statistics for the intensity distribution inside the contour. To eliminate the need for re-initialization and accelerate the curve evolution, we propose a new *SPF* function which we term Global Signed Region Pressure Force (*GSRPF*) function, which can accurately modulate the signs of the pressure forces inside and outside the ROIs.

This paper is organized as follows. In Section 2 we discuss previous global active contour models. Section 3 presents the mathematical formulation of the proposed model and its numerical implementation. Section 4 presents the experimental results comparing the *GSRPF* with known models in the literature on segmentation accuracy based on a number of synthetic and real images. Finally, Section 5 offers conclusions.

978-1-4673-5807-1/13/$31.00 ©2013 IEEE DSP2013

II. Discussion of Previous ACMs

In this section, to appreciate the contribution of the proposed model we briefly review two widely used global region-based active contour models.

A. Chan-Vese ($C-V$) Model

The ($C-V$) model [8], the classical region-based model, uses the region's statistical information to construct a region stopping function that can stop the contour evolution between different regions. The level set formulation of the $C-V$ model, regarding the time evolution of the level set function ϕ, can be described as

$$\frac{\partial \phi}{\partial t} = \delta(\phi)\left[\mu \nabla(\nabla \phi / |\nabla \phi|) - v - \lambda_1 (I(x) - c_1)^2 + \lambda_2 (I(x) - c_2)^2\right], \quad (1)$$

where, $I(x)$ denotes an image indexed by pixel location x, $\mu \geq 0$, v increases the propagation speed, $\lambda_1 \geq 0$, and $\lambda_2 \geq 0$ are parameters that control the influence of each term. The first term keeps the level set function smooth, while the second and third terms are the internal and external forces respectively that drive the contour towards the object boundaries, and $\delta(\phi)$ is the Dirac function. c_1 and c_2 are defined as follows:

$$c_1 = \frac{\int_\Omega I(x) \cdot H(\phi)\, dx}{\int_\Omega H(\phi)\, dx}, \quad (2)$$

$$c_2 = \frac{\int_\Omega I(x) \cdot (1 - H(\phi))\, dx}{\int_\Omega (1 - H(\phi))\, dx}, \quad (3)$$

where, $H(\phi)$ is the Heaviside function and Ω is the image domain.

Plainly described the $C-V$ model drives the contour (towards a smooth solution) to enclose regions that maximize the difference in their average intensity. Overall, compared to *GAC* models that rely on edge gradients the $C-V$ model is less sensitive to initialization and can recognize the object's boundaries efficiently. Furthermore, the implementation of this model requires the re-initialize of the evolution curve to be a signed distance function, which is computationally expensive operation.

B. Selective Binary and Gaussian Filtering Regularized (SBGFRLS) Model

The *SBGFRLS* model [10] combines the advantages of the $C-V$ and *GAC* models. It utilizes the statistical information inside and outside the contour to construct a region-based signed pressure force (*SPF*) function, which is used in place of the edge stopping function (ie., the information related to image gradients) in the *GAC* model. Its level set formulation can be described as

$$\frac{\partial \phi}{\partial t} = spf(I(x)) \cdot \alpha |\nabla \phi|, \quad (4)$$

where, α is the balloon force parameter (controlling the rate expansion of the level set function) and the spf is defined as

$$spf(I(x)) = \frac{I(x) - \frac{c_1 + c_2}{2}}{max\left(\left|I(x) - \frac{c_1 + c_2}{2}\right|\right)}, \quad (5)$$

where, c_1 and c_2 are defined in Eqs. 2 and 3. Observe that compared to the $C-V$ model, in Eq. 1 here the Dirac function $\delta(\phi)$ has been replaced by $|\nabla \phi|$ which according to the authors has an effective range of the whole image, rather than the small range of the Dirac functional. Also, the bracket in Eq. 1 is replaced by the spf function defined in Eq. 5. To regularize the curve the authors in [10] (following the practice of others, e.g., [3], [10], [16]), rather than relying on the computationally costly $\mu \nabla(\nabla \phi / |\nabla \phi|)$ term, they convolve the level set curve with a Gaussian kernel (K_σ), ie.,

$$\phi = K_\sigma \circ \phi. \quad (6)$$

This σ controls the interface of the curve as μ does in Eq. 1 of the $C-V$ model. If the value of σ is small, then the level set function is sensitive to the noise and it does not allow the level set function to flow into the narrow regions of the object.

Overall this model is faster, computationally efficient, and performs better than the conventional $C-V$ model as pointed in [10].

III. The Proposed Model

The majority of global intensity based active contour models (as reviewed in the previous section) assume that regions of interest are composed by flat homogeneous (in intensity) regions. Consequently, when these assumptions are violated the performance of these models is far from the desired.

We propose a new intensity driven model that can efficiently model the foreground (ie., the object(s)) when they are characterized by a non symmetric distribution. This non symmetry could arise either from intensity variations or from the fact that the object could be composed by two or more intensity classes. To provide a computationally efficient solution and reduce the possibility of trapping into local minima we provide an *SPF*-like formulation (which we term *GSRPF*).

A. Model Description

It is obvious that relying only on the global mean (inside and outside the contour as in $C-V$ model is not sufficient when describing intensity distributions when images have foregrounds with more complex intensity distributions. To overcome this problem, we minimize the segmentation energy by introducing the global median in addition to the global mean. Assuming a contour C, x a pixel location in the image $I(x)$, the energy term is defined as

$$E^G(C, c^+, m^+, c^-) = \int_{in(C)} \lambda^+ e^+(x) dx + \int_{out(C)} 2\lambda^- e^-(x) dx \quad (7)$$

$$e^+(x) = \left|I(x) - c^+\right|^2 + \left|I(x) - m^+\right|^2, \quad (8)$$

$$e^-(x) = \left|I(x) - c^-\right|^2, \quad (9)$$

where, λ^+ and λ^- define the weight of each term (inside and outside the contour), c^+ and m^+ are the scalar approximations of the mean and median respectively for image I inside the contour, and c^- is the scalar approximation of the mean outside the contour. Following standard level set formulations [8] we replace the contour curve C with the level set function ϕ [17]

$$E^G\left(\phi, c^+, m^+, c^-\right) = \int_{\phi \succ 0} \lambda^+ e^+(x) dx + \int_{\phi \prec 0} 2\lambda^- e^-(x) dx. \tag{10}$$

The statistical descriptors c^+, m^+, and c^- now can be defined in similar fashion to other intensity driven active contour models as statistical averages and medians

$$\begin{cases} \vec{c^+}(\phi) = \text{average}(I \in \phi(x) \succeq 0), \\ \vec{m^+}(\phi) = \text{median}(I \in \phi(x) \succeq 0), \\ \vec{c^-}(\phi) = \text{average}(I \in \phi(x) \prec 0), \end{cases} \tag{11}$$

Using the level set function ϕ to represent the contour C in the domain Ω, the energy functional can be written as follows:

$$E^G\left(\phi, c^+, m^+, c^-\right) = \int_\Omega \lambda^+ e^+(x) H(\phi(x)) dx + \int_\Omega 2\lambda^- e^-(x)(1 - H(\phi(x))) dx, \tag{12}$$

where H is the Heaviside function.

By keeping c^+, m^+, and c^- fixed, we minimize the energy function $E^G(\phi, c^+, m^+, c^-)$ with respect to ϕ to obtain the gradient descent flow as

$$\frac{\partial \phi}{\partial t} = \delta(\phi)\left[-\lambda^+ e^+(x) + 2\lambda^- e^-(x)\right], \tag{13}$$

where δ is the Dirac delta function.

By considering the higher order statistics, our model can overcome the limitation of the $C-V$ model as a symmetric statistical assumption, which is not accurate most of the real-life images. In the binary gray level images, our model as an energy minimization model behaves exactly the same as $C-V$ model where $m^+ = c^+$. However, by having our model as a *GSRPF*, implementation with *SPF* function, it is still more robust to the initialization than $C-V$ in handling binary gray images.

B. The GSRPF sign pressure function formulation

Although we could rely on Eq. 13 to update our level set, obtaining an 'SPF' like formulation would reduce the possibility of trapping into the local minimum by well modulating the interior and exterior forces.

In this section we propose such formulation which we term Globally Signed Region Pressure Force (*GSRPF*) function. It is derived such that it can modulate the signs of the pressure force inside and outside the object of interest using the statistical quantities defined in Eq. 11 and the minimization of the proposed energy functional of Eq. 13.

First, we assume $\lambda^+ = \lambda^- = 1$, then we define the *SPF* function as follows:

$$spf(I(x)) \quad = \quad spf_1 \cdot spf_2(I(x)), \tag{14}$$

where,

$$\begin{cases} spf_1 = sign(2c^+ + 2m^+ - 4c^-), \\ spf_2(I(x)) = sign(I(x) - \frac{c^{+2} + m^{+2} - 2c^{-2}}{2c^+ + 2m^+ - 4c^-}), \end{cases} \tag{15}$$

where, c^+, m^+, and c^- are defined in Eq. 11.

Rather than a constant force (the α in Eq. 4), we use a force that is a quadratic function of $I(x)$ to control the propagation of the evolving curve

$$\alpha(I(x)) = \left(I(x) - \frac{c^{+2} + m^{+2} - 2c^{-2}}{2c^+ + 2m^+ - 4c^-}\right)^2. \tag{16}$$

The significance of the proposed propagation function $\alpha(I(x))$ is to dynamically increase the interior and exterior forces of the curve when it is far from the boundaries (thus reducing the possibility of entrapment in local minimal) and decrease the forces when the curve is close to the boundaries (thus allowing the curve to stop very close to the actual boundaries).

The (per-pixel) multiplication of the proposed $\alpha(I(x))$ and $spf(I(x))$ results in a new region-based signed pressure force function, which we term Globally Signed Region Pressure Forces (*GSRPF*):

$$gsrpf(I(x)) = \alpha(I(x)) \cdot spf(I(x)). \tag{17}$$

The proposed *GSRPF* has the capacity to modulate the sign of the pressure forces and implicitly control the propagation of the evolving curve so that the contour shrinks when it is outside the object of interest and expands when it is inside the object.

Following the spf formulation in section II-B the final level set formulation of our model is:

$$\frac{\partial \phi}{\partial t} = gsrpf\left(I(x)\right) \cdot |\nabla \phi|. \tag{18}$$

For computational efficiency, as in section II-B, we use a Gaussian kernel to regularize the level set function to keep the interface regular. The σ of the smoothing kernel is the only control parameter of the model.

As we will demonstrate in the results section the proposed model:

- is capable of identifying objects of complex intensity distribution (by considering the skewness of the distribution);
- is robust to additive noise (e.g. a higher order statistics is considered in our model to accommodate the non symmetric and noisy distributions);
- is not sensitive to initialization (since only global information is considered for the curve evolution);
- is computationally efficient (since it does not require re-initialization of the level set function and regularizes the contour efficiently); and
- requires few iterations to converge.

C. Implementation

To illustrate the ease of implementation of our model, the main steps of the algorithm can be summarized as:

1) Initialize the level set function ϕ to be binary as follows:

$$\phi(x,t=0)=\begin{cases} -\rho & x\in\Omega_0-\Omega_0^{'} \\ 0 & x\in\Omega_0^{'} \\ \rho & x\in\Omega-\Omega_0 \end{cases} \tag{19}$$

where $\rho \succ 0$ is a constant, Ω_0 is a subset in the image domain Ω and $\Omega_0^{'}$ is the boundary of Ω_0;
2) Calculate the GSRPF with Eq. 17;
3) Evolve the level set according to Eq. 18;
4) Regularize the level set according to Eq. 6;
5) If the curve evolution has converged, stop and return the result. Otherwise return to Step 2.

IV. Experimental Results

In this section we demonstrate the superiority of the proposed method, compared to reference implementations of the methods proposed in Section II, when presented with challenging synthetic and real images. We implemented the proposed algorithm in Matlab R2009b on a PC (2.5-GHz Intel(R) Core(TM) 2 Duo, 2.00 GB RAM). For fair comparison we used reference Matlab implementations of the $C-V$ and *SBGFRLS*.

To demonstrate the effectiveness of our approach in handling images where the background has multiple intensity classes we created a synthetic image for this purpose shown in Fig. 1, without additive noise and with noise. We compare the performance of the proposed model with the $C-V$ and *SBGFRLS* models, and vary the parameters. As Fig. 1(a) illustrates, by increasing the value of σ, the proposed *GSRPF* is less sensitive to the noise and finds all the regions of the object for a large span of σ. On the other hand, the *SBGFRLS* model (Fig. 1(d)) is not able to evolve properly through the noisy regions even when altering the values of α and σ values. Similarly, as Fig. 1(e) shows, the $C-V$ model is unable to segment the image with different μ values.

To demonstrate the accuracy of the proposed method quantitatively we adopt the precision and recall metrics, and compare the algorithms result with the ground truth. Fig. 2 shows the effect of σ on the accuracy of the segmentation result using the synthetic image with noise shown in Fig. 1(a) using the ground truth. Based on this experiment, $\sigma = 1.4$ is recommended to handle noisy images with multiple classes in the foreground.

Table I shows the robustness of our model when different levels of noise is added to the synthetic image of Fig. 1. The high precision at most noise levels confirms the ability of the proposed *GSRPF* to find all the regions of the object irrespective of noise strength.

Fig. 3(b) illustrates the ability of the *GSRPF* model to find accurately the boundaries of objects with various convexities, shapes, and noisy background. *SBGFRLS* can identify the objects, however, it is unable to segment the hole inside the object, as shown in Fig. 3(c). The $C-V$ model is unable to segment this image (as shown in Fig. 3(d)) because $C-V$ model is trapped into the local minima.

To demonstrate the speed and adaptability of the proposed function, in Fig. 4 we show the curve evolution for a few iterations. It is readily evident that our model converges fast to an accurate delineation of the foreground object.

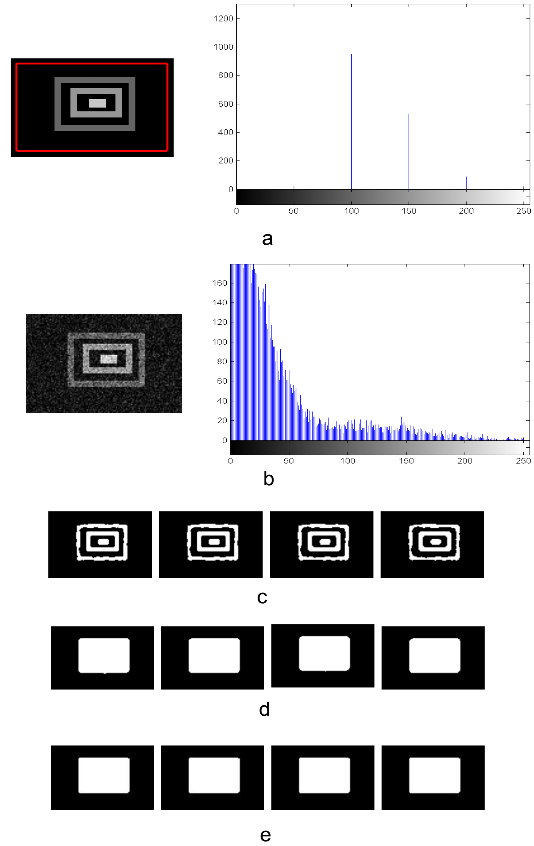

Fig. 1: A synthetic image with multiple classes in the foreground and the performance of the proposed, *SBGFRLS*, and $C-V$, models as a function of their parameters. (a) the original 123 x 80 image with three different intensities 100, 150 and 200, and its histogram; (b) the same image with Gaussian noise added of standard deviation (SD) 30, and its histogram. Overlaid also is the initial contour (in red) used in all subsequent tests. From left to right the segmentation results in (c) of our model with different σ values (1.4, 1.6, 1.8, and 2); (d) of *SBGFRLS* with different σ and α values ((2,10), (2,50), (2.5, 10), and (2.5,50) respectively); and (e) of the $C-V$ model with different μ values (1.4, 1.6, 1.8, and 2).

TABLE I: The robustness of *GSRPF* model ($\sigma = 1.4$) to noise level: the precision and recall with different Gaussian noise levels controlled by standard deviation (*SD*).

SD	10	20	30	40	50
Precision(%)	100	100	100	99	89
Recall (%)	10	99	89	80	71

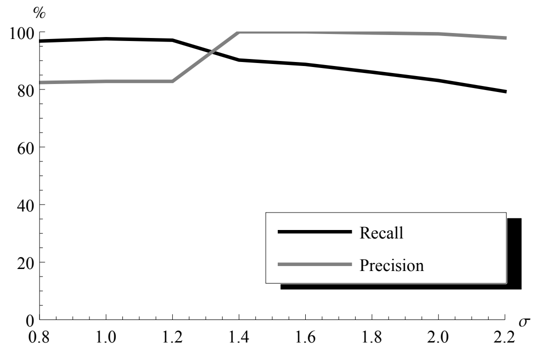

Fig. 2: The sensitivity of our model to the parameter σ, in segmenting the image in Fig. 1 with Gaussian noise, SD = 30, in terms of Recall and Precision.

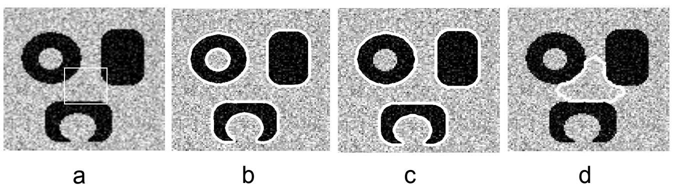

Fig. 3: The segmentation results on a 101 x 99 synthetic image containing different objects of variable convexity and shape, and noisy background. Left to right: the original image (with the initial contour), proposed ($\sigma = 1.4$), *SBGFRLS*, and $C-V$ models.

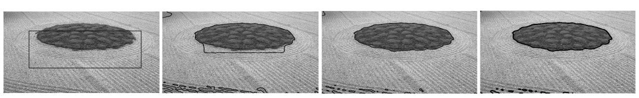

Fig. 4: Demonstrating the rapid evolution of the proposed model ($\sigma = 3.5$) on a 481 x 321 real image (downloaded from [18]). Left to right: initial contour, contour at 6 and 9 iterations, and final contour (15 iterations).

Fig. 5 shows the robustness of the proposed *GSRPF* model but the sensitivity of the *SBGFRLS* and $C-V$ models to different contour initializations. The interior and exterior forces are accurately defined independent of the initial contour's location. The initial position of the contour does not affect the final segmentation, as Fig. 5(b), (f), (j), and (n) show, and the presence of the plane's shadow does not lead to over-segmentation. On the other hand, the *SBGFRLS* model is unable to accurately segment the object when the contour is initialized outside the object, as shown in Fig. 5(g), (k), and (o). On the other hand, the $C-V$ model is more robust to the initialization compared to *SBGFRLS*, with the exception of Fig. 5(p).

Fig. 6 demonstrates the ability of our method in handling images arising in the life and natural sciences. In Fig. 6(a) all models accurately delineate the boundaries of a brain malignancy. Fig. 6(b) shows the ability of our model to extract accurately an Arabidopsis rosette from a complicated background (e.g. soil, pot, tray); however, the other two

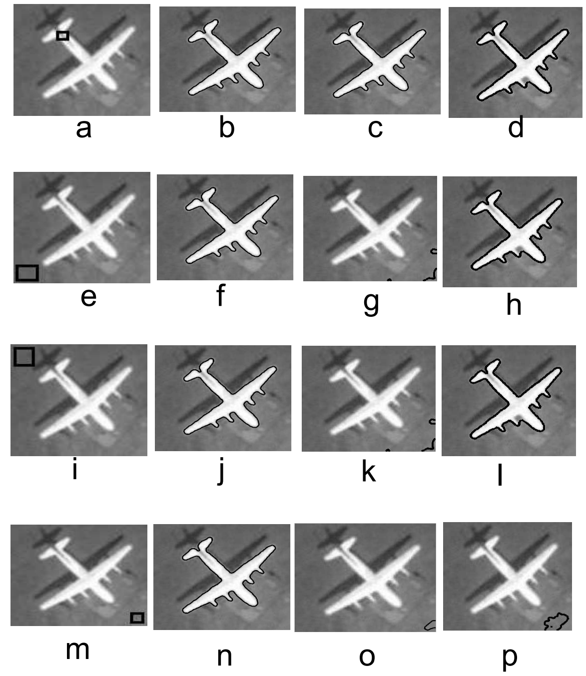

Fig. 5: Testing robustness to initialization when segmenting a 135 x 125 plane image obtained from [19]. Arranged as columns are the original image with different contour initializations, and then from left to right the results of the proposed *GSRPF* ($\sigma = 1.4$), *SBGFRLS* (with $\sigma = 1$ and $\alpha = 25$), and $C-V$ (with $\mu = 0.2$) models respectively, when using the same initial contour.

models are not able to extract all the plant parts, as seen in Fig. 6(c) and 6(d). Similarly, Fig. 6(c) and (d) show the ability of *GSRPF* to segment multiple objects in the scene, such as cells and chromosomes. On the other hand the segmentation results of the *SBGFRLS* and $C-V$ models are not satisfactory. This is mainly attributed to the fact that both models impose certain conditions on the foreground intensity distribution, and as such they cannot minimize the overlap between the object and background distributions.

To demonstrate the computational efficiency of the proposed method when compared to other global methods, Table II shows the CPU time in seconds and final number of iterations (to convergence) for all the images used here. Overall it is able to segment the images in roughly half the number of iterations when compared to *SBGFRLS*, another spf-like model.

V. Conclusion

In this paper, we proposed a novel energy based-active contour model based on a new Globally Signed Region Pressure Force (*GSRPF*) function. *GSRPF* considers the global information extracted from an ROI and accommodates also foreground intensity distributions that are not necessarily symmetric. It automatically and efficiently modulates the signs of the pressure forces inside and outside the contour. The resulting algorithm is less sensitive to noise, contour initialization, and can handle images with complexity in the foreground

TABLE II: The CPU time and number of iterations required by the proposed *GSRPF*, *SBGFRLS*, and $C-V$ models to segment the foreground in some of the images used here.

Figure	GSRPF		SBGFRLS		C-V	
	CPU Time(s)	Iterations	CPU Time(s)	Iterations	CPU Time(s)	Iterations
Fig. 3(a)	0.06	11	0.12	17	-	-
Fig. 5(a)	0.56	21	0.82	45	4.89	339
Fig. 6(a)	.03	10	.05	13	1.5	75
Fig. 6(b)	4.02	46	7.58	84	82.89	806
Fig. 6(c)	1.93	41	2.79	67	16.36	406
Fig. 6(d)	0.92	29	-	-	-	-

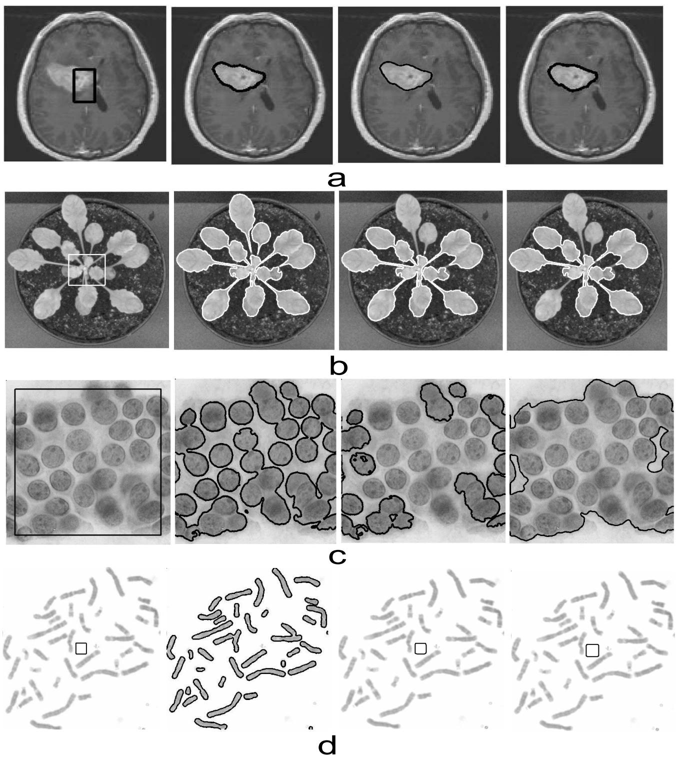

Fig. 6: Segmentation results when different real images encountered in the life or natural sciences are used. Arranged as rows are: (a) a 109 x 119 brain MRI image, from [20]; (b) a 436 x 422 Arabidopsis optical image with complex background; (c) a 256 x 256 cellulose microscopy image, from [21]; and (d) a 256 x 256 chromosome microscopy image, from [21]. Arranged as columns are the original image (with the initial contour), and then from left to right the results of the proposed *GSRPF*, *SBGFRLS*, and $C-V$ models respectively, when using the same initial contour. (Parameters as in Fig. 5, except (a) of *GSRPF* ($\sigma = 1$)).

and/or background. Our model is a Gaussian regularizing level set model that relies only on a single parameter. It is designed to have a quadratic behavior to converge in a few iterations without penalizing segmentation accuracy. Results on synthetic and real images from a variety of scenarios demonstrate the superiority of our model in segmentation accuracy when compared with well regarded global level set methods, such as the *SBGFRLS* [10] and $C-V$ [8] models.

References

[1] V. Caselles, R. Kimmel, and G. Sapiro, "Geodesic Active Contours," *International Journal of Computer Vision*, vol. 22, no. 1, pp. 61–79, Feb. 1997.

[2] S. Kichenassamy, A. Kumar, and P. Olver, "Conformal Curvature Flows: From Phase Transitions to Active Vision," 1995.

[3] G. Zhu, "Boundary-based image segmentation using binary level set method," *Optical Engineering*, vol. 46, no. 5, pp. 050 501+, May 2007.

[4] N. Paragios and R. Deriche, "Geodesic active contours and level sets for the detection and tracking of moving objects," *Pattern Analysis and Machine Intelligence, IEEE Transactions on*, vol. 22, no. 3, pp. 266–280, Mar. 2000.

[5] C. Xu and J. L. Prince, "Snakes, Shapes, and Gradient Vector Flow," in *IEEE Transactions on Image Processing*, 1998, pp. 359–369.

[6] A. Vasilevskiy and K. Siddiqi, "Flux Maximizing Geometric Flows," in *IEEE Transactions on Pattern Analysis and Machine Intelligence*, 2001, pp. 1565–1578.

[7] C. Li, C. Xu, C. Gui, and M. D. Fox, "Level set evolution without re-initialization: A new variational formulation," in *in Proc. of IEEE Conference on Computer Vision and Pattern Recognition*, 2005, pp. 430–436.

[8] T. F. Chan and L. A. Vese, "Active contours without edges," *Image Processing, IEEE Transactions on*, vol. 10, no. 2, pp. 266–277, Feb. 2001.

[9] L. Chen, Y. Zhou, Y. Wang, and J. Yang, "GACV: Geodesic-Aided CV method," *Pattern Recognition*, vol. 39, no. 7, pp. 1391–1395, Jul. 2006.

[10] K. Zhang, L. Zhang, H. Song, and W. Zhou, "Active contours with selective local or global segmentation: A new formulation and level set method," *Image and Vision Computing*, vol. 28, no. 4, pp. 668–676, Apr. 2010.

[11] L. Wang, L. He, A. Mishra, and C. Li, "Active contours driven by local Gaussian distribution fitting energy," *Signal Processing*, vol. 89, no. 12, pp. 2435–2447, Dec. 2009.

[12] P. Wang, K. Sun, and Z. Chen, "Local and Global Intensity Information Integrated Geodesic Model for Image Segmentation," in *Computer Science and Electronics Engineering (ICCSEE), 2012 International Conference on*, vol. 2. IEEE, Mar. 2012, pp. 129–132.

[13] T.-T. Tran, V.-T. Pham, Y.-J. Chiu, and K.-K. Shyu, "Active contour with selective local or global segmentation for intensity inhomogeneous image," in *Computer Science and Information Technology (ICCSIT), 2010 3rd IEEE International Conference on*, vol. 1. IEEE, Jul. 2010, pp. 306–310.

[14] U. Vovk, F. Pernus, and B. Likar, "A Review of Methods for Correction of Intensity Inhomogeneity in MRI," *Medical Imaging, IEEE Transactions on*, vol. 26, no. 3, pp. 405–421, Mar. 2007.

[15] S. Liu and Y. Peng, "A local region-based ChanVese model for image segmentation," *Pattern Recognition*, vol. 45, no. 7, pp. 2769–2779, Jul. 2012.

[16] Y. Shi and W. C. Karl, "Real-time tracking using level sets," in *Computer Vision and Pattern Recognition, 2005. CVPR 2005. IEEE Computer Society Conference on*, vol. 2. IEEE, Jun. 2005, pp. 34–41 vol. 2.

[17] H.-K. Zhao, T. Chan, B. Merriman, and S. Osher, "A Variational Level Set Approach to Multiphase Motion," *Journal of Computational Physics*, vol. 127, no. 1, pp. 179–195, 1996.

[18] http://www.eecs.berkeley.edu/Research/Projects/CS/vision/bsds/.

[19] http://www4.comp.polyu.edu.hk/ cskhzhang/.

[20] http://www.unc.edu/ liwa/.

[21] http://decsai.ugr.es/cvg/dbimagenes/gbio256.php.